Synthesis of triple stranded porphyrin nanobelts

Authors: Arnau Rodríguez-Rubio,[1]† He Zhu,[1]† Ka Man Cheung,[1]† Igor Rončević,[2] Lene A. Gödde,[1] Janko Hergenhahn,[1] Joshua L. Field,[1] Prakhar Gupta,[1] Wojciech Stawski,[3] Henrik Gotfredsen,[1] Joseph Straw,[4] Matthew Edmondson,[4] James N. O'Shea,[4] Alex Saywell,[4]* and Harry L. Anderson[1]*

Affiliations:

[1] Department of Chemistry, Oxford University, Chemistry Research Laboratory, Oxford, United Kingdom.

[2] Department of Chemistry, The University of Manchester, Oxford Road, Manchester, United Kingdom.

[3] Institute of Organic Chemistry II and New Materials, Ulm University, Albert-Einstein-Allee 11, 89081 Ulm, Germany.

[4] School of Physics & Astronomy, University of Nottingham, Nottingham, United Kingdom

† These authors contributed equally

*Corresponding author. Email: harry.anderson@chem.ox.ac.uk, alex.saywell@nottingham.ac.uk

Abstract: Molecular nanobelts are fascinating analogues of carbon nanotubes. Their rigid geometries and strongly coupled π-electrons have the potential to generate a wavefunction resembling that of a quantum ring. Here we report the synthesis of triple-stranded nanobelts consisting of 8 to 12 edge-fused porphyrin units with diameters of 21 to 32 Å. These nanobelts were synthesized by nickel-mediated coupling of *meso*-bromoporphyrins, to form singly-linked nanorings, followed by oxidation with gold(III) chloride. Experimental ^{1}H NMR spectra, supported by computational simulations, reveal that belts containing odd numbers of porphyrins, with circuits of 90 or 110 π-electrons, display global aromatic ring currents, whereas even-numbered belts, with 80, 100 or 120 π-electrons, are globally antiaromatic.

One-Sentence Summary: Edge-fused porphyrin nanobelts exhibit global (anti)aromatic ring currents, for circuits of up to 120 π-electrons even in the neutral molecules.

Main Text:

Single-walled carbon nanotubes adopt three main structural types: zigzag, armchair and chiral. Very short hydrogen-terminated sections of these tubes are known as carbon nanobelts (*1-3*). Hypothetical benzenoid nanobelts have been discussed for decades (*4*), but until recently all attempts at synthesizing them failed, due to their high strain and reactivity. Now, several viable synthetic approaches have been developed (*5-11*) leading to intense interest in their potential as optoelectronic materials (*12,13*) and as hosts for supramolecular recognition (*8,11*). The simplest type of benzenoid nanobelt, and the first to be considered theoretically, are the [*n*]cyclacenes (Fig. 1A) (*1,4*). These simple zigzag belts are calculated to have open-shell singlet biradical ground states (*14*), reflecting their lack of Clar sextets (*15*), and this property seems to make them too reactive to isolate. So far, they have only been detected by mass spectrometry (*16*). The biradical character of [*n*]cyclacenes can be suppressed by building in extra benzene rings along the rims of the belt, so that every carbon atom of the π-system becomes part of a Clar sextet (Fig. 1B) (*8,9*). One of the most interesting features of a molecular nanobelt is extreme electronic delocalization, potentially making the electronic wavefunction resemble that of a particle on a ring (i.e., a quantum ring) (*17,18*), yet paradoxically, all reported syntheses of benzenoid nanobelts (e.g. Fig. 1C,D) target nanobelts with many Clar sextets, thus reducing electronic delocalization and increasing chemical stability. All benzenoid nanobelts constructed from six-membered rings are alternant hydrocarbons. Including five-membered rings results in a non-alternant structure and tends to increase the electronic delocalization (*19-21*).

Here we present the synthesis of a family of edge-fused porphyrin nanobelts (***cf*-P*N***, Fig. 1E). The presence of hetero-atoms and five-membered rings in these nanobelts results in highly delocalized non-alternant structures. Furthermore, these porphyrin nanobelts are triple-stranded (meaning that at least three bonds must be cut to cleave the ring), which amplifies the electronic coupling around the circumference. Previously reported non-porphyrin nanobelts have been double-stranded (*1-3,22*). The electronic delocalization in the neutral edge-fused porphyrin nanobelts is evidenced in their ^{1}H NMR spectra, which reveal strong global ring currents. Nanobelts with odd and even numbers of porphyrin units have diatropic (aromatic) and paratropic (antiaromatic) global ring currents, respectively, in keeping with Hückel's 4*n*+2 rule and with previously published theoretical predictions (*23*). Another manifestation of the strong global π-conjugation is that the electronic absorption spectra of the neutral nanobelts extend far into the infrared, with intense peaks in the region 1500–2000 nm. Previously reported porphyrin-based nanobelts have bridging units separating the porphyrins, rather than direct porphyrin-porphyrin coupling, they do not exhibit global ring currents (*22,24-26*), and they do not have such red-shifted absorption spectra.

Nanoring synthesis by nickel-mediated coupling. The edge-fused porphyrin nanobelts reported here are cyclic analogues of the porphyrin nanoribbons pioneered by Tsuda and Osuka (*27*). Previous work has shown that these linear ribbons exhibit exceptionally wire-like charge transport (*28-30*), implying that they are promising components for the construction of molecular quantum rings (*18*). Linear porphyrin nanoribbons are synthesized by oxidative fusion of singly-linked porphyrin chains (*27-32*), so the obvious precursors to edge-fused porphyrin nanobelts are singly-linked porphyrin nanorings (***cs*-P*N***). We explored various template-directed strategies for preparing the required singly-linked rings, without success (*33-35*). Then, much to our surprise, we found that they are formed serendipitously, together with linear polymers, during the Yamamoto coupling of nickel(II) 5,15-dibromoporphyrins (*28*) (Fig. 2).

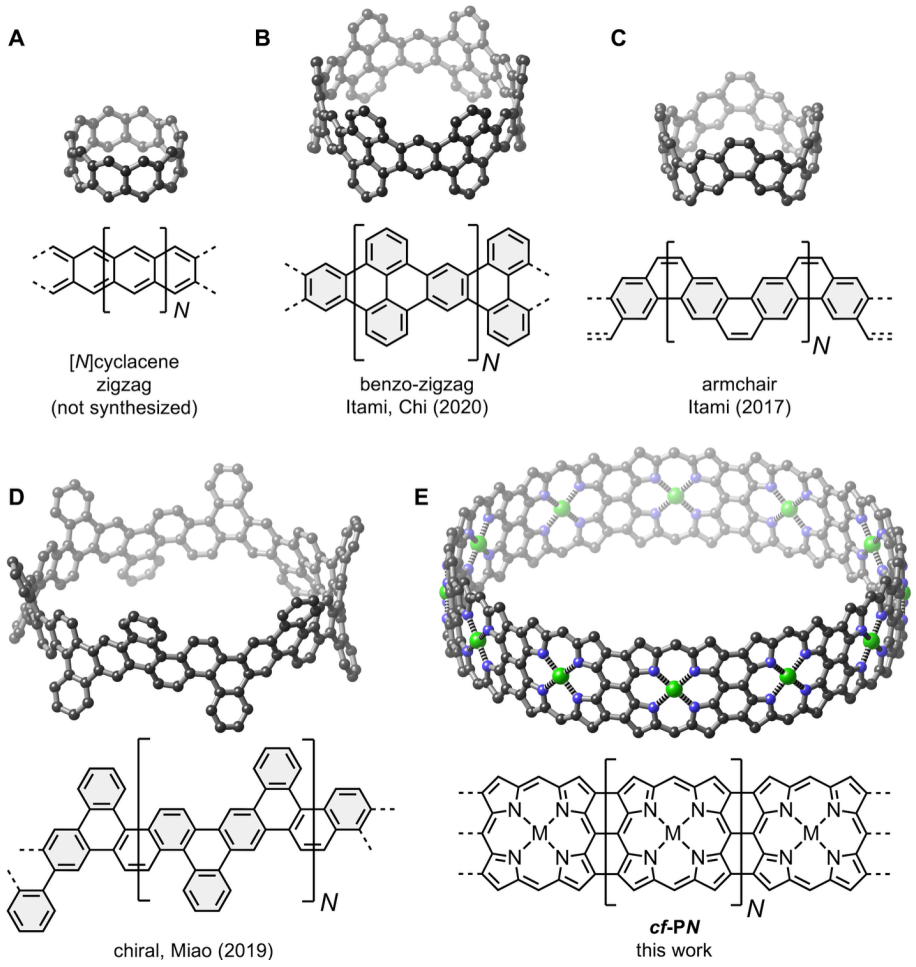

Fig. 1. Comparison of molecular nanobelts. A [*N*]cyclacene, **B** benzo[*N*]cyclacene, **C** armchair nanobelt, **D** chiral nanobelt, **E** edge-fused porphyrin nanobelt. The projections of the 3D structures are all shown on the same scale. Clar sextets are shaded gray in **B**, **C** and **D**.

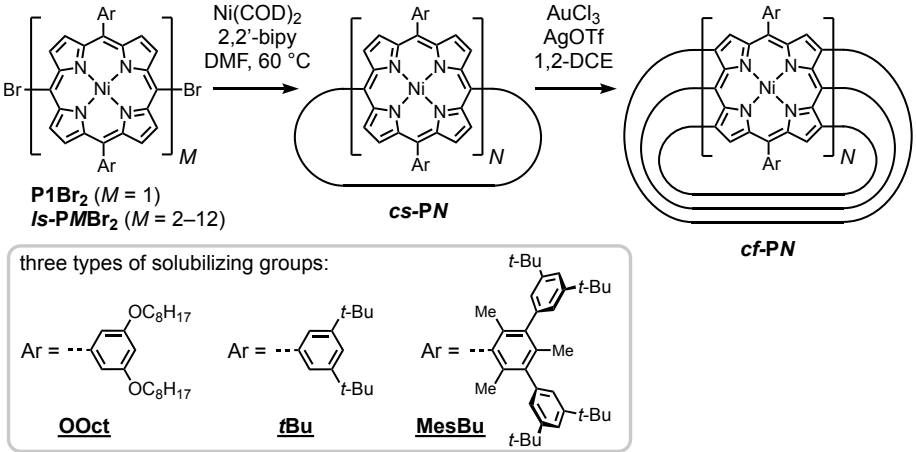

Fig. 2. Synthetic route to porphyrin nanobelts. *M* and *N* are the numbers of porphyrin units in the starting material and rings, respectively. Solubilizing groups are denoted with subscripts; for example the three monomers have compound codes $\mathbf{P1}_{\mathbf{OOct}}\mathbf{Br}_2$, $\mathbf{P1}_{\mathbf{tBu}}\mathbf{Br}_2$ and $\mathbf{P1}_{\mathbf{MesBu}}\mathbf{Br}_2$. The prefixes ***ls***, ***cs*** and ***cf*** denote "linear singly-linked", "cyclic singly-linked" and "cyclic fused". (Abbreviations: COD = 1,5-cyclooctadiene; 2,2′-bipy = 2,2′-bipyridine; DMF = dimethylformamide; 1,2-DCE = 1,2-dichloroethane; Ar = aryl; OTf = trifluoromethanesulfonate)

The Yamamoto coupling reaction shown in Fig. 2 was carried out, starting from a dibromo nickel(II) porphyrin monomer **P1Br$_2$** or a linear singly-linked oligomer ***ls*-P*M*Br$_2$** (where *M* is the number of porphyrin units), to obtain the cyclic singly-linked oligomers ***cs*-P*N*** with a distribution of ring sizes. These reactions were performed using porphyrins with three different aryl solubilizing groups (OOct, tBu or MesBu, as defined in Fig. 2). The singly-linked rings ***cs*-P*N*** were separated by gel permeation chromatography (GPC) and isolated for $N = 6$ to 12. (Small amounts of larger rings up to $N = 24$ were also detected, but have not yet been fully characterized.) Cyclic oligomers have longer GPC retention times than linear chains with the same numbers of porphyrin units (*36*), and the first evidence for the cyclic nature of ***cs*-P*N*** came from a combination of GPC and mass spectrometry. For example, the GPC trace of a crude reaction mixture from the cyclooligomerization of ***ls*-P2$_{OOct}$Br$_2$** is shown in Fig. 3A, together with the traces of the isolated products ***cs*-P6$_{OOct}$**, ***cs*-P8$_{OOct}$**, ***cs*-P10$_{OOct}$** and ***cs*-P12$_{OOct}$**. The isolated yields of the cyclic oligomers are plotted as a function of ring size, for various precursors, in Fig 3B. The small number of signals in the ^{1}H NMR spectra of ***cs*-P*N*** oligomers was consistent with the formation of highly symmetric cyclic molecules, without end-groups, and this was confirmed by scanning tunneling microscopy (STM). For example, Fig. 3C shows an STM image of ***cs*-P8$_{OOct}$**, recorded under vacuum after electrospray deposition onto a gold surface (octyloxy-substituted porphyrin polymers are compatible with electrospray deposition and STM imaging on gold surfaces (*34*-*36*)). Steric repulsion between β-hydrogen atoms results in a severe twist between neighboring porphyrin units in singly *meso*-*meso*-linked oligomers (*37*), which explains why the STM image of ***cs*-P8$_{OOct}$** has 4-fold (rather than 8-fold) symmetry (see Supplementary Material, fig. S24–S26, for more images of ***cs*-P8$_{OOct}$**, ***cs*-P12$_{OOct}$** and ***cs*-P18$_{OOct}$**).

Suitable crystals of ***cs*-P8$_{tBu}$** for single-crystal x-ray crystallography were grown by diffusion of acetone vapor into a solution of the macrocycle in 1,2-dichlorobenzene (see Supplementary Material for details). There are two crystallographically distinct ***cs*-P8$_{tBu}$** units in the crystal, both with similar conformations, one of which is shown in Fig. 3D. The mean Ni–Ni diameter is 20.65(0.66) Å. As expected, the macrocycle has a highly twisted geometry and neighboring porphyrin units are almost orthogonal. The average angle between the 24-atom planes of neighboring porphyrins is 84.4(2.7)° and the angle between the porphyrin units and the mean plane of the eight Ni centers is 48.6(6.2)°.

It is surprising that Yamamoto coupling of 5,15-substituted nickel(II) porphyrins gives cyclic oligomers, in the absence of any template. Coupling the corresponding zinc(II) porphyrin derivatives under identical conditions only yields linear oligomers (see Supplementary Material, fig. S9). One reason why nickel(II) porphyrins favor the formation of cyclic products is that they tend to adopt non-planar geometries, because the N-Ni bond length is too short for the cavity of the porphyrin (*38*). This distortion of the porphyrin units reduces the strain in ***cs*-P*N*** rings when metalated with Ni rather than Zn, as confirmed by density functional theory (DFT) calculations (see Supplementary Material, fig. S30). For example, we calculate that ***cs*-P16** is almost unstrained when metallated with Ni (strain energy 4.9 kJ mol^{-1}), whereas it has a strain energy of 116.8 kJ mol^{-1} when metalated with Zn.

Another factor that probably favors formation of cyclic products is that nickel(II) porphyrins are electron-deficient (*39*), which is expected to retard the reductive elimination step in Yamamoto coupling (*40*). This could lead to the formation of cyclic C_{meso}-Ni-C_{meso} linked intermediates, in which all the C-Br bonds are replaced by C-Ni-C links before reductive elimination occurs (fig. S31). In other words, metalation of the porphyrins with nickel favors a mechanism in which

macrocyclization occurs before reductive elimination. Similar organo-nickel intermediates have been used in the synthesis of cycloparaphenylenes consisting of electron-deficient fluorinated *para*-phenylene units (*41*), and in the synthesis of a nanotube end-cap (*42*). Strong support for this hypothesis comes from the observation that coupling ***ls*-P*M*Br$_2$** only gives ***cs*-P*N*** with $N > M$. For example, ***cs*-P6$_{OOct}$** can be prepared by coupling ***ls*-P2$_{OOct}$Br$_2$** but not from ***ls*-P6$_{OOct}$Br$_2$**, demonstrating that the linear hexamer ***ls*-P6$_{OOct}$Br$_2$** is not an intermediate in the formation of the cyclic hexamer ***cs*-P6$_{OOct}$** from ***ls*-P2$_{OOct}$Br$_2$** (see fig. S7b). Similarly, coupling of ***ls*-P12$_{OOct}$Br$_2$** does not give ***cs*-P12$_{OOct}$** (fig. S8). Reversible formation of C_{meso}-Ni-C_{meso} links might allow equilibration between linear and cyclic intermediates, which could also favor macrocyclization.

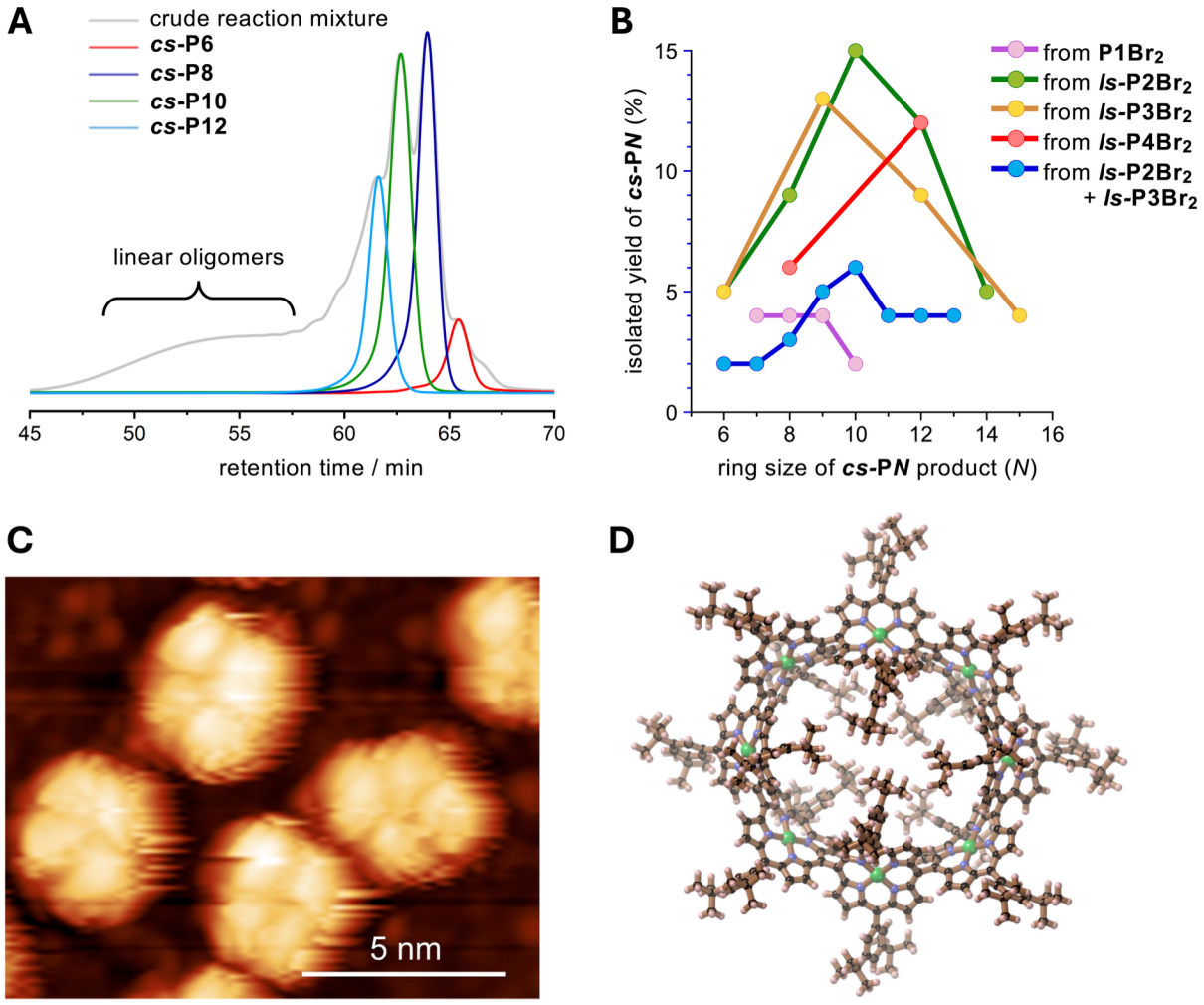

Fig. 3. Synthesis and characterization of singly-linked porphyrin nanorings. (**A**) Gel permeation chromatography (GPC) trace of the crude reaction mixture from Yamamoto coupling of the dibromodimer ***ls*-P2$_{OOct}$** superimposed on traces of isolated cyclic oligomers for $N = 6$, 8, 10 and 12. (**B**) Isolated yields of ***cs*-P*N*$_{OOct}$** ($N = 6$–15) obtained from a range of different starting materials. **(C)** STM image of ***cs*-P8$_{OOct}$** on a Au(111) surface, deposited by electrospray (imaging parameters: sample bias = –2 V, set-point current = 9 pA). (**D**) Single crystal x-ray structure of ***cs*-P8$_{tBu}$**, showing one of two distinct molecular units in the crystal.

Oxidation to nanobelts and global aromaticity. Oxidation of the singly-linked rings ***cs*-P*N*** to the triply-linked nanobelts ***cf*-P*N*** was achieved with gold(III) chloride and silver triflate, in around 95% yield using reaction conditions developed for the synthesis of linear porphyrin ribbons (*28,30,43*). The role of the silver salt is to suppress formation of chlorinated byproducts

(*43*). This fusion reaction is accompanied by a dramatic change in the UV-vis-NIR absorption spectra, and the products exhibit intense absorption bands at 1500–2000 nm (Fig. 4). We tested this chemistry with all three aryl (Ar) groups shown in Fig. 2, and similar UV-vis-NIR spectra were recorded in all three cases, but sharp well resolved ^{1}H NMR spectra were only obtained for ***cf*-P*N*$_{\mathbf{MesBu}}$**, so we focused on this family of nanobelts (N = 8 to 12). We attribute the broadness of the ^{1}H NMR spectra of ***cf*-P*N*$_{\mathbf{OOct}}$** and ***cf*-P*N*$_{\mathbf{tBu}}$** to dynamic rotation of the aryl groups (which is blocked by the *ortho*-methyl groups in ***cf*-P*N*$_{\mathbf{MesBu}}$**) and aggregation (which is hindered by the bulk of the MesBu groups). The ^{1}H NMR spectra of the five ***cf*-P*N*$_{\mathbf{MesBu}}$** nanobelts (Fig. 5) were assigned using a combination of two-dimensional NMR techniques (see Supplementary Materials for details). It was not possible to distinguish between mesityl methyl groups facing inside (Me_{in}) or outside (Me_{out}) of the nanobelts using NOE correlations. We assigned these resonances by assuming that the signal most shielded, or most deshielded, by the global ring current is Me_{in} (*44*). This assignment was fully confirmed by the excellent correlation between experimental chemical shifts and those calculated using DFT (fig. S15). The ^{1}H NMR spectra show dramatic changes in the chemical shifts of the Me_{in}, Me_{out} and β signals, which alternate for odd/even numbers of porphyrin units, indicating that ***cf*-P9$_{\mathbf{MesBu}}$** and ***cf*-P11$_{\mathbf{MesBu}}$** are globally aromatic whereas ***cf*-P8$_{\mathbf{MesBu}}$**, ***cf*-P10$_{\mathbf{MesBu}}$** and ***cf*-P12$_{\mathbf{MesBu}}$** are globally antiaromatic, as predicted (*23*), consistent with the nucleus-independent chemical shift (NICS) plots on the right of Fig. 5. The ring current susceptibilities of the nanobelts with N = 8 to 12 were estimated from the experimental ^{1}H NMR shifts in Me_{in} and Me_{out} using the Biot-Savart law (*18*), giving values of 41.9, –29.8, 31.3, –20.0 and 17.2 nA/T, respectively (compared with –11.8 nA/T in benzene (*45*)). The integrated bond currents in ***cf*-P8** and ***cf*-P9**, calculated using SYSMOIC (*46*) (fig. S16), are similar in magnitude to ring currents from Biot-Savart law analysis, with about 90% of the current flowing through the C_{meso}-C_{meso} bonds, as predicted for the corresponding zinc complexes (*23*).

The UV-vis-NIR absorption spectra of aromatic compounds generally feature sharp intense bands, whereas antiaromatic compounds tend to give broader absorption spectra that tail into the NIR region (*47*). We do not observe a dramatic difference between the absorption spectra of the nanobelts in the series ***cf*-P8$_{\mathbf{MesBu}}$** to ***cf*-P12$_{\mathbf{MesBu}}$**, but there is an alternation in the shape of the NIR spectra between even and odd nanobelts: the aromatic belts ***cf*-P9$_{\mathbf{MesBu}}$** and ***cf*-P11$_{\mathbf{MesBu}}$** exhibit a pattern of sharp shoulder bands at 1700–1900 nm, which is absent in the antiaromatic belts ***cf*-P8$_{\mathbf{MesBu}}$**, ***cf*-P10$_{\mathbf{MesBu}}$** and ***cf*-P12$_{\mathbf{MesBu}}$** (Fig. 4).

In conclusion, we present the synthesis of molecular nanobelts consisting of 8 to 12 edge-fused porphyrin units. The ^{1}H NMR spectra of these neutral compounds reveal that they sustain global ring currents that are diatropic (aromatic) for odd numbers of porphyrins and paratropic (antiaromatic) for even numbers of porphyrins. These findings are in stark contrast with the behavior of previously reported nanobelts (and butadiyne-linked porphyrin nanorings) which only exhibit global ring currents when oxidized or reduced (*18,20,21,44*). The observation of global (anti)aromatic ring currents in neutral porphyrin nanobelts demonstrates that the electronic wavefunction resembles, to some extent, that of a particle on a ring (i.e. a quantum ring) (*18,48*), which implies that charge-transport through these molecules can be controlled by quantum interference. For example, theoretical work indicates that ***cf*-P*N*** nanobelts could function as Aharonov–Bohm-type interferometers (*49*), enabling transport to be controlled by applying a magnetic field.

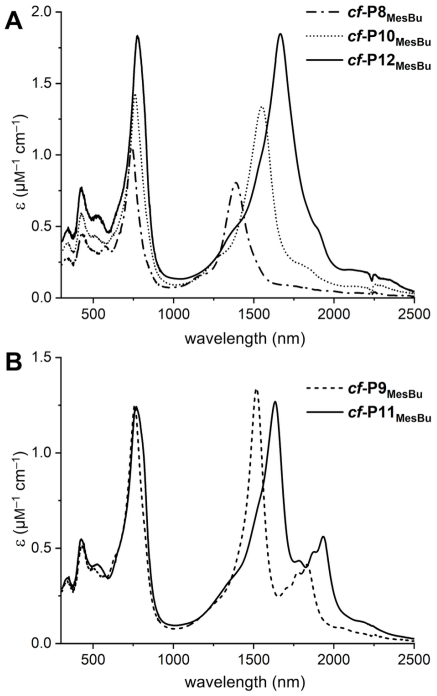

Fig 4. UV-vis-NIR spectra of nanobelts recorded in toluene-d_8. (**A**) Antiaromatic belts with even numbers of porphyrin units. (**B**) Aromatic belts with odd numbers of porphyrin units.

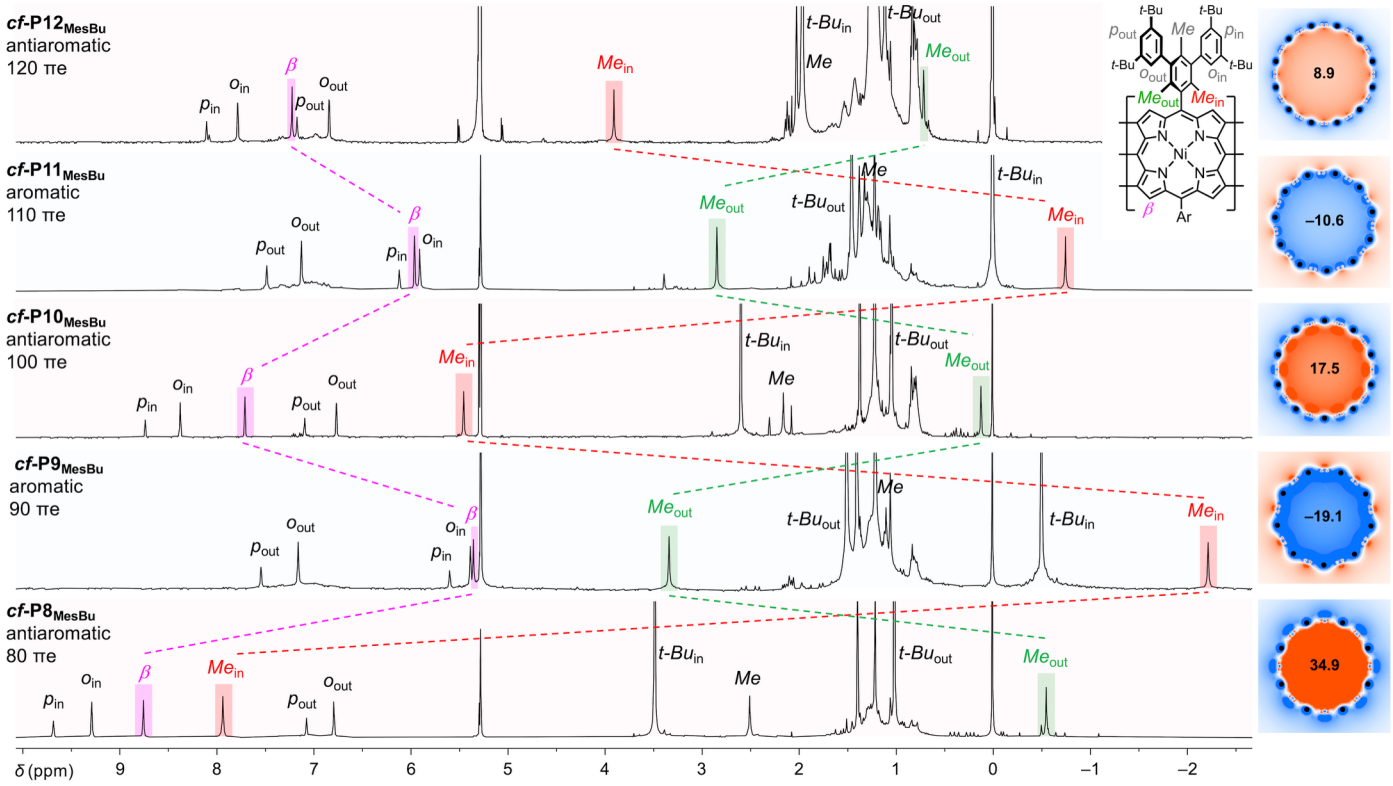

Fig. 5. ^{1}H NMR spectra of porphyrin nanobelts *cf*-P8$_{MesBu}$ – *cf*-P12$_{MesBu}$ recorded in CD_2Cl_2/CS_2 (400 MHz, 298 K). Plots of the nucleus independent shift (NICS) in the plane of the porphyrin for each ring size are shown on the right (NICS(0)$_{zz}$ from DFT calculations the OX-B3LYP/def2-SVP level of theory (*23*). Numbers denote the NICS value at the center of the ring.)

References

1. Q.-H. Guo, Y. Qiu, M.-X. Wang, J. F. Stoddart, Aromatic hydrocarbon belts. *Nat. Chem.* **13**, 402–419 (2021).

2. D. Imoto, A. Yagi, K. Itami, Carbon nanobelts: Brief history and perspective. *Precis. Chem.* **1**, 516–523 (2023).

3. R. Zhang, D. An, J. Zhu, X. Lu, Y. Liu, Carbon nanorings and nanobelts: Material Syntheses, molecular architectures, and applications. *Adv. Funct. Mater.* **33**, 2305249 (2023).

4. E. Heilbronner, *Helv. Chim. Acta* **37**, 921–935 (1954).

5. G. Povie, Y. Segawa, T. Nishihara, Y. Miyauchi, K. Itami, Synthesis of a carbon nanobelt. *Science* **356**, 172–175 (2017).

6. G. Povie, Y. Segawa, T. Nishihara, Y. Miyauchi, K. Itami, Synthesis and size-dependent properties of [12], [16], and [24]carbon nanobelts. *J. Am. Chem. Soc.* **140**, 10054–10059 (2018).

7. K. Y. Cheung, S. Gui, C. Deng, H. Liang, Z. Xia, Z. Liu, L. Chi, Q. Miao, Synthesis of armchair and chiral carbon nanobelts. *Chem* **5**, 838–847 (2019).

8. H. M. Bergman, G. R. Kiel, R. C. Handford, Y. Liu, T. D. Tilley, Scalable, divergent synthesis of a high aspect ratio carbon nanobelt. *J. Am. Chem. Soc.* **143**, 8619–8624 (2021).

9. K. Y. Cheung, K. Watanabe, Y. Segawa, K. Itami, Synthesis of a zigzag carbon nanobelt. *Nat. Chem.* **13**, 255–259 (2021).

10. Y. Han, S. Dong, J. Shao, W. Fan, C. Chi, Synthesis of a sidewall fragment of a (12,0) carbon nanotube. *Angew. Chem. Int. Ed.* **60**, 2658–2662 (2021).

11. Z. Xia, S. H. Pun, H. Chen, Q. Miao, Synthesis of zigzag carbon nanobelts through Scholl reactions. *Angew. Chem. Int. Ed.* **60**, 10311–10318 (2021).

12. J. Lin, S. Wang, F. Zhang, B. Yang, P. Du, C. Chen, Y. Zang, D. Zhu, Highly efficient charge transport across carbon nanobelts. *Sci. Adv.* **8**, eade4692 (2022).

13. M. Ball, B. Zhang, Y. Zhong, B. Fowler, S. Xiao, F. Ng, M. Steigerwald, C. Nuckolls. Conjugated macrocycles in organic electronics. *Acc. Chem. Res.* **52**, 1068−1078 (2019).

14. E. Clar, The aromatic sextet; Wiley: London, 1972.

15. Z. Chen, D.-e. Jiang, X. Lu, H. F. Bettinger, S. Dai, P. von Ragué Schleyer, K. N. Houk, Open-shell singlet character of cyclacenes and short zigzag nanotubes. *Org. Lett.* **9**, 5449−5452 (2007).

16. T.-H. Shi, Q.-H. Guo, S. Tong, M.-X. Wang, Toward the synthesis of a highly strained hydrocarbon belt. *J. Am. Chem. Soc.* **142**, 4576–4580 (2020).

17. M. Solà, F. M. Bickelhaupt, Particle on a ring model for teaching the origin of the aromatic stabilization energy and the Hu̇ckel and Baird rules. *J. Chem. Educ.* **99**, 3497−3501 (2022).

18. M. Jirásek, H. L. Anderson, M. D. Peeks, from macrocycles to quantum rings: Does aromaticity have a size limit? *Acc. Chem. Res.* **54**, 3241−3251 (2021).

19 C. Liu, M. E. Sandoval-Salinas, Y. Hong, T. Y. Gopalakrishna, H. Phan, N. Aratani, T. S. Herng, J. Ding, H. Yamada, D. Kim, D. Casanova, J. Wu, Macrocyclic polyradicaloids with unusual super-ring structure and global aromaticity. *Chem* **4**, 1586–1595 (2018).

20. X. Lu, T. Y. Gopalakrishna, Y. Han, Y. Ni, Y. Zou, J. Wu, Bowl-shaped carbon nanobelts showing size-dependent properties and selective encapsulation of C_{70}. *J. Am. Chem. Soc.* **141**, 5934–5941 (2019).

21. Y. Han, S. Wu, K. Y. S. Khoo, C. Chi, Synthesis of fully π-conjugated non-alternant carbon nanobelts. *Nat. Synth.* (2025). https://doi.org/10.1038/s44160-025-00797-5.

22. R. Haver, H. L. Anderson, Synthesis and properties of porphyrin nanotubes. *Helv. Chim. Acta* **102**, e1800211 (2019).

23. M. Vitek, J.-R. Deng, H. L. Anderson, I. Rončević, Global aromatic ring currents in neutral porphyrin nanobelts. *ACS Nano* **19**, 1405−1411 (2025).

24. J. Song, N. Aratani, H. Shinokubo, A. Osuka, A porphyrin nanobarrel that encapsulates C_{60}. *J. Am. Chem. Soc.* **132**, 16356–16357 (2010).

25. P. Neuhaus, A. Cnossen, J. Q. Gong, L. M. Herz, H. L. Anderson, A molecular nanotube with three-dimensional π-conjugation. *Angew. Chem. Int. Ed.* **54**, 7344–7348 (2015).

26. S. Xue, D. Kuzuhara, N. Aratani, H. Yamada, Synthesis of a porphyrin(2.1.2.1) nanobelt and its ability to bind fullerene. *Org. Lett.* **21**, 2069−2072 (2019).

27. A. Tsuda, A. Osuka, *Science* **293**, 79–82 (2001).

28. H. Zhu, G. Wen, W. Zheng, N. H. Rees, W. Stawski, H. I. Wang, M. Bonn, H. L. Anderson, High charge carrier mobility in porphyrin nanoribbons. *Angew. Chem. Int. Ed.* **64**, e202417429 (2025).

29. S. M. Kopp, J.-R. Deng, A. J. Redman, H. Gotfredsen, R. M. J. Jacobs, H. L. Anderson, C. R. Timmel, Cationic polaron delocalization in porphyrin nanoribbon. *Chem* **10**, 3595–3606 (2024).

30. J.-R. Deng, M. T. González, H. Zhu, H. L. Anderson, E. Leary, Ballistic conductance through porphyrin nanoribbons. *J. Am. Chem. Soc.* **146**, 3651–3659 (2024).

31. T. Ikeda, N. Aratani, A. Osuka, Synthesis of extremely π-extended porphyrin tapes from hybrid *meso-meso* linked porphyrin arrays: An approach towards the conjugation length. *Chem. Asian J.* **4**, 1248–1256 (2009).

32. T. Tanaka, A. Osuka, Triply linked porphyrinoids. *Chem. Eur. J.* **24**, 17188–17200 (2018).

33. J. M. Van Raden, J.-R. Deng, H. Gotfredsen, J. Hergenhahn, M. Clarke, M. Edmondson, J. Hart, J. N. O'Shea, F. Duarte, A. Saywell, H. L. Anderson, Template-directed synthesis of strained *meso*-*meso*-linked porphyrin nanorings. *Angew. Chem. Int. Ed.* **63**, e202400103 (2024).

34. M. A. Majewski, W. Stawski, J. M. Van Raden, M. Clarke, J. Hart, J. N. O'Shea, A. Saywell, H. L. Anderson, Covalent template-directed synthesis of a spoked 18-porphyrin nanoring. *Angew. Chem. Int. Ed.* **62**, e202302114 (2023).

35. H. Gotfredsen, J.-R. Deng, J. Van Raden, M. Righetto, J. Hergenhahn, M. Clarke, A. Bellamy-Carter, J. Hart, J. O'Shea, T. D. W. Claridge, F. Duarte, A. Saywell, L. M. Herz, H. L. Anderson, Bending a photonic wire into a ring. *Nat. Chem.* **14**, 1436–1442 (2022).

36. D. V. Kondratuk, L. M. A. Perdigão, A. M. S. Esmail, J. N. O'Shea, P. H. Beton, H. L. Anderson, Supramolecular nesting of cyclic polymers. *Nat. Chem.* **7**, 317–322 (2015).

37. N. Aratani, A. Takagi, Y. Yanagawa, T. Matsumoto, T. Kawai, Z. S. Yoon, D. Kim, A. Osuka, Giant *meso–meso*-linked porphyrin arrays of micrometer molecular length and their fabrication. *Chem. Eur. J.* **11**, 3389–3404 (2005).

38. X.-Z. Song, W. Jentzen, S.-L. Jia, L. Jaquinod, D. J. Nurco, C. J. Medforth, K. M. Smith, J. A. Shelnutt, Representation of nonplanar structures of nickel(II) 5,15-disubstituted porphyrins in terms of displacements along the lowest-frequency normal coordinates of the macrocycle. *J. Am. Chem. Soc.* **118**, 12975–12988 (1996).

39. D. G. Davis, "Electrochemistry of porphyrins" in *The Porphyrins*, D. Dolphin, Ed., vol. V (Academic Press, 1978), pp. 127–152.

40. T. Yamamoto, Y. Murakami, M. Abla, Control of reductive elimination and acidolysis of diarylnickel(II) complexes by the kind of Brønsted acid and the presence of oxygen. *Chem. Lett.* **28**, 419–420 (1999).

41. H. Shudo, M. Kuwayama, M. Shimasaki, T. Nishihara, Y. Takeda, N. Mitoma, T. Kuwabara, A. Yagi, Y. Segawa, K. Itami, Perfluorocycloparaphenylenes. *Nat. Commun.* **13**, 3713 (2022).

42. D. Myśliwiec, M. Kondratowicz, T. Lis, P. J. Chmielewski, M. Stępień, M. Highly strained nonclassical nanotube end-caps. A single-step solution synthesis from strain-free, non-macrocyclic precursors. *J. Am. Chem. Soc.* **137**, 1643–1649 (2015).

43. A. K. Sahoo, Y. Nakamura, N. Aratani, K. S. Kim, S. B. Noh, H. Shinokubo, D. Kim, A. Osuka, Synthesis of brominated directly fused diporphyrins through gold(III)-mediated oxidation. *Org. Lett.* **8**, 4141–4144 (2006).

44. M. Jirásek, M. Rickhaus, L. Tejerina, H. L. Anderson, Experimental and theoretical evidence for aromatic stabilization energy in large macrocycles. *J. Am. Chem. Soc.* **143**, 2403−2412 (2021).

45. H. Fliegl, D. Sundholm, S. Taubert, J. Jusélius, W. Klopper, Magnetically induced current densities in aromatic, antiaromatic, homoaromatic, and nonaromatic hydrocarbons. *J. Phys. Chem. A* **113**, 8668–8676 (2009).

46. G. Monaco, F. F. Summa, R. Zanasi, Program package for the calculation of origin-independent electron current density and derived magnetic properties in molecular systems. *J. Chem. Inf. Model.* **61**, 270–283 (2021).

47. J. Oh, Y. M. Sung, Y. Hong, D. Kim, Spectroscopic diagnosis of excited-state aromaticity: capturing electronic structures and conformations upon aromaticity reversal. *Acc. Chem. Res.* **51**, 1349−1358 (2018).

48. M. Solà, F. M. Bickelhaupt, Particle on a ring model for teaching the origin of the aromatic stabilization energy and the Hückel and Baird rules. *J. Chem. Educ.* **99**, 3497−3501 (2022).

49. C. Y. Cheng, G. Harari, I. Rončević, J. E. Peralta, H. L. Anderson, A. M. Wibowo-Teale, O. Hod, Molecular Aharonov–Bohm-type interferometers based on porphyrin nanorings. *Chem. Sci.* **16**, 4392–4401 (2025).

50. I. Rončević, H. L. Anderson, J. Hergenhahn, Supplementary computational data for triple stranded porphyrin nanobelts. Zenodo: 10.5281/zenodo.15675187 (2025).

51. K. M. Cheung, A. Rodríguez-Rubio, H. Zhu, H. L. Anderson, Supplementary experimental data for triple stranded porphyrin nanobelts. Zenodo: 10.5281/zenodo.16738579 (2025).

52. C.-M. Feng, Y.-Z. Zhu, Y. Zang, Y.-Z. Tong, J.-Y. Zheng, Switchable regioselectivity in the PIFA–BF_3·Et_2O mediated oxidative coupling of *meso*-brominated Ni(II) porphyrin. *Org. Biomol. Chem.* **12**, 6990–6993 (2014).

53. T. Yamamoto, S. Wakabayashi, K. Osakada, Mechanism of C-C coupling reactions of aromatic halides, promoted by $Ni(COD)_2$ in the presence of 2,2′-bipyridine and PPh_3, to give biaryls. *J. Organomet. Chem.* **428**, 223–237 (1992).

54. M. J. Frisch, G. W. Trucks, H. B. Schlegel, et al., Gaussian 16, Revision A.03 (2016).

55. D. Bansal, D. Cardenas-Morcoso, N. Boscher, N. Conjugated porphyrin polymer films with nickel single sites for the electrocatalytic oxygen evolution reaction. *J. Mater. Chem. A* **11**, 5188–5198 (2023).

56. C. Berríos, G. I. Cárdenas-Jirón, J. F. Marco, C. Gutiérrez, M. S. Ureta-Zañartu, Theoretical and spectroscopic study of nickel(II) porphyrin derivatives. *J. Phys. Chem. A*, **111**, 2706–2714 (2007).

57. L. Palatinus and G. Chapuis, Superflip – a computer program for the solution of crystal structures by charge flipping in arbitrary dimensions. *J. Appl. Crystallogr.* **40**, 786–790 (2007).

58. G. M. Sheldrick, Crystal structure refinement with SHELXL. *Acta Crystallogr.* **C71**, 3–8 (2015).

59. O. V. Dolomanov, L. J. Bourhis, R. J. Gildea, J. A. K. Howard and H. Puschmann, OLEX2: a complete structure solution, refinement and analysis program. *J. Appl. Crystallogr.* **42**, 339–341 (2009).

60. J. P. Perdew, M. Ernzerhof, K. Burke, Rationale for mixing exact exchange with density functional approximations. *J. Chem. Phys.* **105**, 9982–9985 (1996).

61. F. Weigend, R. Ahlrichs, Balanced basis sets of split valence, triple zeta valence and quadruple zeta valence quality for H to Rn: Design and assessment of accuracy. *Phys. Chem. Chem. Phys.* **7**, 3297–3305 (2005).

62. R. Haver, L. Tejerina, H.-W. Jiang, M. Rickhaus, M. Jirasek, I. Grübner, H. J. Eggimann, L. M. Herz, H. L. Anderson, Tuning the circumference of six-porphyrin nanorings. *J. Am. Chem. Soc.* **141**, 7965−7971 (2019).

Acknowledgments: We thank Marco Vitek for discussions.

Funding: European Research Council grant 885606, ARO-MAT (HLA, AR-R, KMC, JH, PG and WS).

The Royal Society for a University Research Fellowship (AS).

UKRI Horizon Europe Guarantee MSCA Postdoctoral Fellowship ElDelPath, EP/X030075/1 (IR, HLA).

The Centre for Doctoral Training in Synthesis for Biology and Medicine for a studentship, generously supported by GlaxoSmithKline, MSD, Syngenta and Vertex (JLF).

Author contributions: Conceptualization: HLA, AR-R, HZ and KMC

First serendipitous observation of Yamamoto cyclization: HZ

Synthetic experimental work and spectroscopy: AR-R, HZ, KMC, JLF, HG

Theoretical analysis and computational simulations: IR and JH

Biot-Savart calculations: LAG

X-ray crystallography: PG and WS

Scanning probe microscopy: JS, ME, JO'S and AS

Writing: All authors

Competing interests: The authors declare that they have no competing interests.

Data and materials availability: X-ray data are available free of charge from the Cambridge Crystallographic Data Centre under accession numbers CCDC-2463702 and 2463698. All experimental data are reported in the main text and supplementary materials, as are detailed methods to prepare the reported compounds (*50*,*51*).

Supplementary Materials

Materials and Methods

Supplementary Text

Figs. S1 to S116

Tables S1 to S14

References (*52*–*62*)